Maximum Allowable Current Determination of RBS By Using a Directed Graph Model and Greedy Algorithm

Binghui Xu[1†], Guangbin Hua[1†], Cheng Qian[1*], Quan Xia[1,2], Bo Sun[1], Yi Ren[1], and Zili Wang[1]

[1]School of Reliability and Systems Engineering, Beihang University, Beijing, 100191, China

[2]School of Aeronautic Science and Engineering at Beihang University, Beijing, China

[*]Address correspondence to: cqian@buaa.edu.cn

[†]These authors contributed equally to this work.

Abstract

Reconfigurable battery systems (RBSs) present a promising alternative to traditional battery systems due to their flexible and dynamically changeable topological structure that can be adapted to different battery charging and discharging strategies. During RBS operation, a critical system parameter known as the maximum allowable current (MAC) become pivotal. This parameter is instrumental in maintaining the current of each individual battery within a safe range and serves as a guiding indicator for the system's reconfiguration, thereby ensuring its safety and reliability. This paper proposes a method to calculate the MAC of arbitrary RBSs using a greedy algorithm in conjunction with a directed graph model of the RBS. By introducing the shortest path (SP) of the battery, the greedy algorithm transforms the enumeration of switch states in the brute-force algorithm or variable search without utilizing structures in the heuristic algorithms (simulated annealing and genetic algorithm) into the combination of the shortest paths~~, which greatly increases~~. This significantly enhances the efficiency with which the MAC is determined. The directed graph model, based on the equivalent circuit, provides a specific method for calculating the MAC of a given structure. The proposed method is validated on two published ~~four-battery-RBSs~~ RBS structures and one with a more complex structure. The results are the same as those of the brute-force algorithm, but the proposed method significantly improves the computational efficiency ($N_s 2^{N_s - N_b} \log_{10} N_b$ times faster than the ~~brute-force~~ brute-force algorithm for an RBS with N_b batteries and N_s switches, theoretically). ~~The main~~ Another advantage of the proposed method is its ability to calculate the MAC of RBSs with arbitrary structures and variable battries, even in scenarios with random isolated batteries.

1 Introduction

Battery energy storage systems (BESSs) are ~~extensively used~~ widely utilized in various applications [1], such as wind power plants [2] and space power systems [3, 4], ~~to store and release~~ for the purpose of storing and releasing high-quality electrical energy [5]. Typically, a BESS consists of numerous batteries interconnected by series-parallel circuitry to provide the required ~~capacity storage~~ storage capacity. However, ~~traditional~~ conventional BESSs, in which the batteries are connected in a fixed topology, suffer from a significant weakness in their worst battery due to the so-called cask effect. ~~Moreover~~Furthermore, if the worst battery fails during operation, it is highly likely to ~~exacerbate~~ accelerate the degradation of the other batteries, ~~leading to~~ resulting in reliability and safety issues at the system level [6, 7, 8]. These ~~problems have become significant technical barriers~~ challenges have become major technical obstacles in many engineering projects ~~requiring~~ that demand high reliability, such as ~~developing new-generation~~ the development of next-generation space vehicles [9].

Reconfigurable battery systems (RBSs), which can dynamically switch ~~as required to~~ between different circuit topologies as needed, are expected to ~~solve this problem [10]. The switching circuit helps to isolate unhealthy batteries, thereby improving the safety and reliability of the battery system. To illustrate the working principle of an RBS, we consider~~ address these issues [10]. In a typical RBS~~structure developed by Visairo [11] (Fig. ??), which is taken as an example to show the reconfiguration process. In this structure, the batteries can be connected not only in series when the switches~~ S_1, ~~S_5, S_6, S_7, S_8, S_9, and S_{13} are closed (see Fig. ??) but also in parallel when S_1, S_2, S_3, S_4, S_5, S_9, S_{10}, S_{11}, S_{12}, and S_{13} are closed (Fig. ??). Furthermore, when an unhealthy battery, for instance,~~ additional switches are introduced between the batteries to form a reconfigurable network, where the circuit's topology can be altered by opening or closing the switches. By opening the switches adjacent to the unhealthy batteries, they can be isolated from the system, ensuring that the system remains in a reliable operational state [12]. Furthermore, the ~~orange one~~ ~~B_3 in Fig. ??, appears in the RBS , it can be isolated by opening its two adjacent switches (i.e., S_4 and S_{11}), ensuring that the systemremains in a reliable working mode~~RBS can be reconfigured to adapt to different charging and discharging strategies, thereby enhancing the system's efficiency and prolonging the battery's lifespan [13]. These advantages make RBSs a promising alternative to traditional BESSs.

~~(a) The RBS structure proposed by Visairo[11], with all batteries in (b) series connection, (c) parallel connection, and (d) battery B_3 isolated.~~

~~Recently, various types of RBSs with different~~ The early research on RBSs mainly focused on the topological design of the structure, incorporating different levels of flexibility and reconfigurability ~~have been designed~~ to meet application requirements. For example, Ci et al. [14] proposed an RBS structure that dynamically adjusts the battery discharge rate to fully exploit the available capacity of each battery. Jan's [15, 16] structures reconfigure ~~structures~~ circuits with variant batteries in series to ~~reach the (constantly changing)~~ accommodate the constantly changing voltage requirements during electric vehicle charging. ~~As shown in Fig. ??, the~~ The structure proposed by Visairo et al. [11] ~~changes~~ alters the system's output voltage based on the load conditions, thereby reducing ~~the power loss of~~ power loss in the voltage regulator during the power supply process and ~~improving~~

the efficiency of energy useenhancing energy efficiency. Also, to enhance the energy efficiency of the system, Lawson et al. [17] and He et al. [18] proposed simplified structures that have fewer switches than Visairo's design. Kim et al. [19] improved the system's ability to recover from battery failures by introducing multiple ports into the structure.

The complex structure However, these complex structures between batteries and switches gives RBSs flexibility but also creates challenges in the designand control of the system . Thus, several approaches to analyze the RBS structure and performance have been proposed to tackle these challenges. For instance, provide flexibility to RBSs while also posing challenges in hardware design. During the reconfiguration process, current deviation and fluctuation may occur. Specifically, when the system switches from series to parallel connection, circulating current between parallel cells can be triggered due to voltage imbalance [20]. Failure to fully consider this issue during the design of RBSs can result in damage to the batteries, switches, and wires. For example, Engelhardt et al. [21] applied RBS to a fast-charging scenario with adaptive cell switching, which can balance cell states while adhering to voltage requests. However, the switching of batteries leads to intolerable current variations. To address this problem, Han et al. [22] derived an analytical expression for the maximum switch current during battery system reconfigurationfor a specific RBS structure. This helps guide . This analytical expression aids in the selection of switches and supports the design of RBS hardware. hardware design of RBSs.

Recently, there has been increasing attention given to the estimation and control of the system state of RBSs, and several approaches have been proposed to optimize the performance of the system. State estimation, which is an essential technology in traditional battery management systems, serves as the foundation for system control and holds great potential in the context of RBSs [23]. Couto et al. [24] introduced a partition-based unscented Kalman filter to estimate the state of a large-scale RBS, utilizing an enhanced reduced-order electrochemical model. Kersten et al. [25] utilized the balancing current of neighboring cells in parallel operation to determine battery impedances, thereby obtaining information about the state of health and power capability. Schmid et al. [26] further leveraged the reconfigurable nature of the system to actively diagnose faults, employing an algorithm that changes the system structure to enhance fault isolability. Another active research topic is the development of effective control strategies for RBSs to achieve optimal performance, including improved stability [27] and efficiency [28]. Han et al. [29] proposed a near-fastest battery balancing algorithm to minimize the time required for battery charge equalization. Liu et al. [30] also proposed a scheme for maximizing capacity utilization based on a path planning algorithm, aiming to enhance battery consistency within the system. To break through the bootleneck of the potential short-circuit paths increase exponentially with the RBS's scale, Chen et al. [31] proposed a systematic approach based on sneak circuit theoryto fundamentally avoid the short-circuit problem of RBSs: They thoroughly analyzed . They conducted a comprehensive analysis of all paths between the cathode and anode of each battery in the RBSand identified , identifying paths that only contain consist of switches as short-circuit paths for pre-checking before system reconfiguration. Furthermore, Artificial Intelligence also appears in the RBS management [32]. The effectiveness of deep reinforcement learning method has been validated in real-world RBSs [28].

In spite of the maximum switch current mentioned above, the The maximum allowable cur-

rent (MAC), which is defined as the maximum ~~allowed current under~~ current allowed within the constraints of the battery cell, is ~~another critical~~ a crucial indicator of RBSs that needs to be evaluated during the design ~~or~~ and control of the system. The MAC ~~helps the designers assess~~ assists designers in assessing whether the RBS meets the ~~output current requirements~~ requirements for output current and contributes to the ~~formulation~~ development of appropriate and safe management strategies for the battery management system. Unfortunately, ~~few studies have analyzed the RBS structure to determine the RBS MAC~~ there have been few studies proposed to directly determine the MAC of RBSs, primarily due to the complexity arising from reconfiguration. In the field of computer science, there is a similar problem of scheduling tasks on dynamically reconfigurable hardware with limited resources and task interdependencies, which is analogous to the determination of MAC. A corresponding method has been proposed [33, 34]. However, dealing with the structural characteristics and circuit equations of RBSs is challenging for this method. From the perspective of RBS structure analysis, the MAC problem can be transformed into finding the maximum output current among all possible reconfigurations of the RBS. ~~An intuitive and straightforward method is to enumerate all possible switch states and calculate the output current of the system under each reconfigurated structure.~~ However, this ~~method is inefficient and time-consuming, especially for RBSs with a large number of switches.~~ may be an NP-hard problem [35]. Common methods such as brute-force algorithms, simulated annealing (SA) algorithms, and genetic algorithms (GA) have the drawbacks of inefficiency, time consumption, and inability to guarantee the globally optimal solution.

To solve this issue, this paper proposes an efficient method to evaluate the MAC of RBSs. In this method, a greedy algorithm is designed to efficiently search the possible circuit topology of RBSs with MAC. This algorithm transforms the ~~enumeration of switch states in the brute-force algorithm into the combination of the batteries' shortest paths . An improved direct graph model that considers the voltage, the~~ inefficiently searching reconfigurations into the proactively combining of the shortest paths of batteries. Furthermore, an improved directed graph model is introduced to analyze the current of the RBS, taking into account factors such as voltage, internal resistance, ~~the~~ MAC of the battery, and ~~the external loadis also introduced to analyze the current of the RBS.~~ external load. The main contributions of this ~~paper~~ study can be summarized as follows:

- An efficient method is proposed to determine the MAC of RBSs with arbitrary structures, including scenarios with isolated batteries.
- A greedy algorithm is applied to solve the MAC problem, the computational complexity of which is greatly reduced compared with the brute-force algorithm.
- An improved directed graph model is introduced to provide a specific method for calculating the MAC of a given structure.

The remainder of this paper is organized as follows: Section II presents the framework and details of the proposed directed graph model and greedy algorithm. Section III ~~discusses~~ examines a case study that ~~uses~~ applies the proposed method to determine the MACs of two published ~~four-battery RBSs~~ RBS structures and one with a more complex structure. The calculation re-

sults, the ~~algorithm's computational complexity~~ computational complexity of the algorithm, and scenarios such as battery random isolation are also discussed. Finally, the concluding remarks are presented in Section IV.

2 Methodology

The central principle of this method is to connect the batteries in an RBS in parallel to the extent possible, thereby maximizing the output current of the RBS. To achieve this universally and automatically, the overall process is divided into the four steps shown in Fig. 1. First, a directed graph model is established for subsequent computations. The model not only contains the connected relationships between batteries and switches but also retains the performance parameters of the batteries. Subsequently, based on the equivalent circuit, the MAC problem is transformed into specific objective functions and constraints. The shortest paths (SPs, where additional batteries and switches on the path are penalized as distance) for the batteries are then obtained by using the Dijkstra algorithm to connect the batteries in the RBS in parallel. Finally, a greedy algorithm is used to organize the switches, allowing the batteries to connect via their SPs while satisfying the constraints, resulting in the MAC of the RBS.

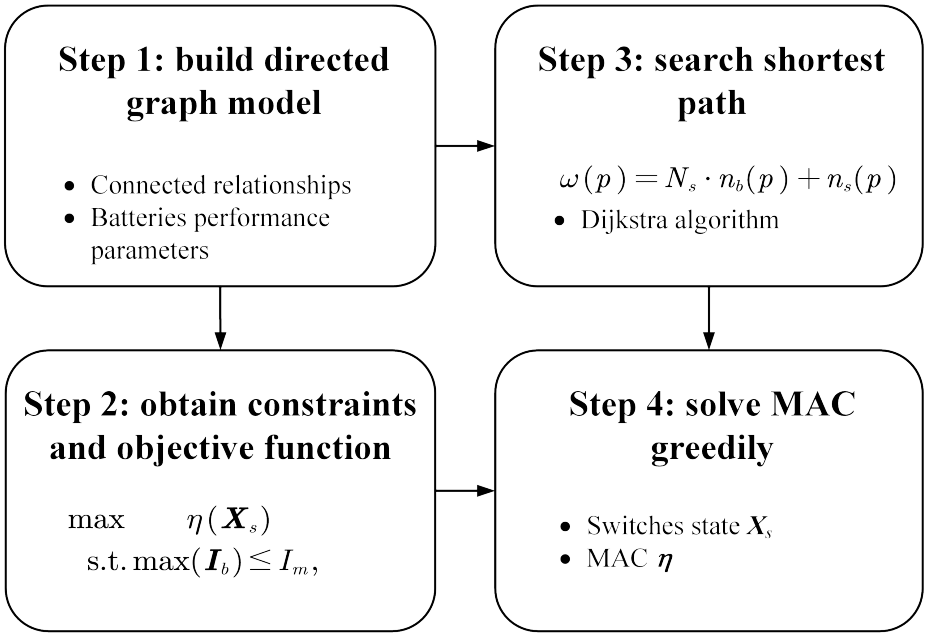

Figure 1: Diagram of this method, which contains four main steps.

2.1 Directed graph model

He et al. [36] proposed an abstracted directed graph model for an RBS, where the nodes represent the batteries, the edges represent the configuration flexibility, and the weight of each vertex corresponds to the battery voltage (Fig. 2a). The model captures all potential system configurations and offers

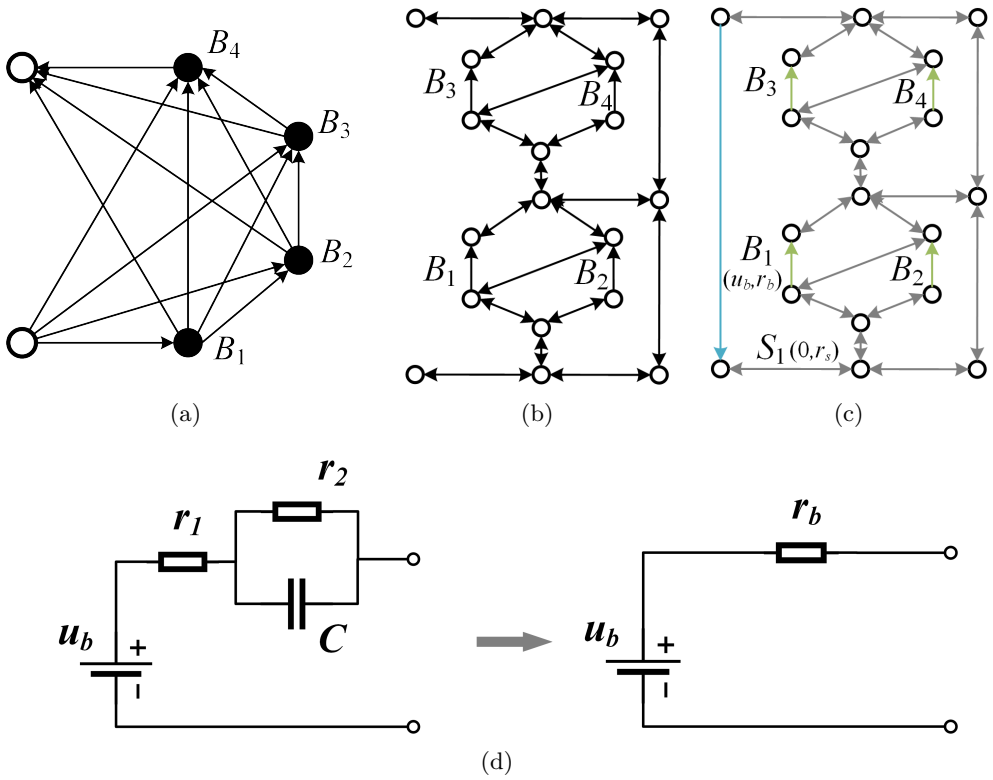

Figure 2: Directed graph models used in (a) He's work [36], (b) our previous work, and (c) the improved model in this paper. (d) The equivalent circuit of a battery in this method.

a direct metric for configuration flexibility, but it does not specify the physical implementation of the connectivity between batteries, meaning that one graph might correspond to multiple RBS structures. We previously proposed a directed graph model that differs completely from He's model by using nodes to represent the connections between batteries and switches and directed edges to represent batteries and switches (Fig. 2b), allowing for a one-to-one correspondence between the RBS structure and the directed graph model. This model accurately and comprehensively represents the RBS topological structure but cannot be used for quantitative MAC calculations because it does not consider the voltage, internal resistance, and MAC of the battery. To address this issue, we improve our previous model by adding electromotive force and resistance attributes on the edges based on its equivalent circuits. The model also considers the external load as an equivalent resistance and integrates it into the analysis, making it a complete circuit model for later circuit analyses. Fig. 2c shows the improved directed graph model used in this paper. The following provides a detailed explanation of the method for equating components in RBSs and constructing the directed graph model.

To use circuit analysis methods to solve the MAC of the RBS, the components in the RBS are equated to ideal circuit elements. For instance, as shown in Fig. 2d, the battery in the RBS is represented as a black-box circuit consisting of two resistors r_1 and r_2 and a capacitor C, known as the Thevenin model [37, 38]. With an emphasis on the stable output of the RBS, the capacitor in the Thevenin model can be considered as an open circuit without affecting the steady-state current. Therefore, battery B_i in the RBS can be simplified as a series connection between a constant voltage source u_i and a resistor r_i. Furthermore, the state of switch S_j in the RBS is represented by a binary variable x_j, where 0 is ON and 1 is OFF. When the switch is closed, the circuit can be regarded as a resistor with a very small resistance r_j. Finally, the external load is considered as a resistor with resistance R_o.

For a given RBS structure, its directed graph model $G(V, E)$ is constructed as follows:

1. Nodes: The nodes in the directed graph correspond to the connection points of components in the actual RBS. Assuming there are a total of N nodes in the RBS, for the sake of convenience, the anode of the RBS is denoted as v_1 and the cathode as v_N.

2. Edges: The edges in the directed graph correspond to the batteries, switches, and external electrical loads in the actual RBS. Therefore, there are three types of directed edges. For battery B_i, its directed edge e_i is drawn from the cathode to the anode because the battery in operation only allows current to flow in one direction. For switch S_j, since it is allowed to work under bidirectional currents, it is represented by a pair of directed edges with two-way directions. Regarding the external electronic load, because it is connected to the anode and cathode of the RBS, a directed edge from v_N to v_1 represents it. In conclusion, for a given RBS structure with N_b batteries and N_s switches, the number of directed edges is $N_b + 2N_s + 1$, where 1 refers to the external electrical load.

3. Attributes of edges: Each edge is assigned two attributes, voltage difference and resistance, based on the equivalent method mentioned above. The values for battery B_i, switch S_j, and external loads correspond to (u_i, r_i), $(0, r_j)$, and $(0, R_o)$, respectively.

2.2 Constraints and objective function

For a given RBS, determining its MAC involves maximizing the RBS output current while ensuring that all battery currents do not exceed the batteries' MAC. This subsection establishes the constraints and objective function to determine the RBS's MAC through circuit analysis based on the directed graph model provided in the previous section.

First, the topology in the directed graph model is represented in matrix form $\boldsymbol{A}$, known as the incidence matrix and defined as follows:

$$a_{kl} = \begin{cases} 1, & \text{edge } l \text{ leaves node } k, \\ -1, & \text{edge } l \text{ enters node } k, \\ 0, & \text{otherwise.} \end{cases} \tag{1}$$

For a directed graph consisting of N nodes and $N_b + 2N_s + 1$ directed edges, its incidence matrix $\boldsymbol{A}$ is an $N \times (N_b + 2N_s + 1)$ matrix. In this matrix, the rows and columns represent the nodes and edges of the directed graph, respectively. By distinguishing the components in the RBS corresponding to each column, $\boldsymbol{A}$ can be rewritten as

$$\boldsymbol{A} = \begin{bmatrix} \boldsymbol{A}_b & \boldsymbol{A}_s & \boldsymbol{A}_o \end{bmatrix}, \tag{2}$$

where $\boldsymbol{A}_b$, $\boldsymbol{A}_s$, and $\boldsymbol{A}_o$ are the submatrices corresponding to the batteries, switches, and external electrical load, respectively. To reduce the computational complexity, the dimensions of matrix $\boldsymbol{A}$ are reduced. Since each directed edge has one node to leave and one to enter, the values in every column of $\boldsymbol{A}$ sum to zero. Therefore, removing the last row will not result in a loss of information. Conversely, since each switch in the RBS is represented by a pair of directed edges with two-way directions, the two columns corresponding to the switch are mutually opposite. Thus, for the submatrix $\boldsymbol{A}_s$, only one column is retained for each pair of columns representing the same switch. As a result, $\boldsymbol{A}$ can be reduced to an $(N-1) \times (N_b + N_s + 1)$ matrix, denoted $\tilde{\boldsymbol{A}}$, for further calculation of current and voltage. Similar to Eq. (2), $\tilde{\boldsymbol{A}}$ can be rewritten as

$$\tilde{\boldsymbol{A}} = \begin{bmatrix} \tilde{\boldsymbol{A}}_b & \tilde{\boldsymbol{A}}_s & \tilde{\boldsymbol{A}}_o \end{bmatrix}. \tag{3}$$

After obtaining the incidence matrix, the currents of all batteries and output in the RBS are determined by solving the circuit equations. According to Kirchhoff's laws, we have

$$\begin{cases} \tilde{\boldsymbol{A}}\boldsymbol{I} = \boldsymbol{0}, \\ \boldsymbol{U} = \tilde{\boldsymbol{A}}^{\mathrm{T}}\boldsymbol{U}_n, \end{cases} \tag{4}$$

where $\boldsymbol{I}$ and $\boldsymbol{U}$ indicate the current and voltage difference arrays of the $N_b + N_s + 1$ edges, respectively, and $\boldsymbol{U}_n$ is the voltage array of the $N-1$ nodes. These directed edges are treated as generalized branches and expressed in matrix form as follows:

$$\boldsymbol{I} = \boldsymbol{Y}\boldsymbol{X}\boldsymbol{U} - \boldsymbol{Y}\boldsymbol{X}\boldsymbol{U}_s + \boldsymbol{I}_s, \tag{5}$$

where $\boldsymbol{U}_s$ and $\boldsymbol{I}_s$ denote the source voltage and source current of the generalized branches, respectively. Because all batteries have been equivalent to voltage sources rather than current sources in the previous subsection, all elements of the array $\boldsymbol{I}_s$ are zero, whereas the elements of the array $\boldsymbol{U}_s$ are equal to the first attribute of the corresponding edges in the directed graph. The matrix $\boldsymbol{Y}$ in Eq. (5) is the admittance matrix of the circuit and is defined as the inverse of the impedance matrix. The elements on the diagonal of matrix $\boldsymbol{Y}$ are equal to the reciprocal of the resistance, which is the second attribute of the corresponding edges in the directed graph. The off-diagonal elements of $\boldsymbol{Y}$ are zero. $\boldsymbol{X}$ is the state matrix that determines whether the RBS batteries and switches can pass current. It is defined as

$$\boldsymbol{X} = \mathrm{diag}(\underbrace{1,0,\ldots,1}_{N_b \text{ of } 0/1},\underbrace{1,0,\ldots,1}_{N_s \text{ of } 0/1},1) = \begin{bmatrix} \boldsymbol{X}_b & & \\ & \boldsymbol{X}_s & \\ & & 1 \end{bmatrix}, \tag{6}$$

where element x_i of matrix $\boldsymbol{X}_b$ indicates whether battery B_i has been removed from the circuit, with $x_i = 1$ indicating removal and $x_i = 0$ indicating that battery B_i is still available to supply power. When all batteries are healthy and capable of providing current to the external load, $\boldsymbol{X}_b$ is the identity matrix. The elements x_j of matrix $\boldsymbol{X}_s$ determine whether switch S_j is closed, with $x_j = 1$ indicating a closed switch and $x_j = 0$ indicating an open switch, which is consistent with the previous subsection.

Theoretically, the output current I_o and the currents of each battery $\boldsymbol{I}_b$ in the RBS can be determined by solving Eqs. (4)–(6) under any given state $\boldsymbol{X}$. To further simplify the problem, it is assumed that all batteries have the same electromotive force and internal resistance, which are denoted u_b and r_b, respectively. This allows us to derive explicit expressions for I_o and $\boldsymbol{I}_b$. After derivation and simplification, the output current I_o and the currents of each battery $\boldsymbol{I}_b$ are ultimately represented as Eqs. (7) and (8), respectively:

$$I_o = \frac{1}{R_o r_b} \tilde{\boldsymbol{A}}_o^{\mathrm{T}} \boldsymbol{Y}_n^{-1}(\boldsymbol{X}) \tilde{\boldsymbol{A}}_b \boldsymbol{U}_b, \tag{7}$$

$$\boldsymbol{I}_b = \frac{1}{r_b^2} [\tilde{\boldsymbol{A}}_b^{\mathrm{T}} \boldsymbol{Y}_n^{-1}(\boldsymbol{X}) \tilde{\boldsymbol{A}}_b \boldsymbol{U}_b - r_b \boldsymbol{U}_b], \tag{8}$$

where $\boldsymbol{U}_b$ is an $N_b \times 1$ array with all elements equal to u_b, and $\boldsymbol{Y}_n$ is the equivalent admittance matrix of the circuit and is defined as

$$\boldsymbol{Y}_n(\boldsymbol{X}) = \frac{1}{R_o} \tilde{\boldsymbol{A}}_o \tilde{\boldsymbol{A}}_o^{\mathrm{T}} + \frac{1}{r_b} \tilde{\boldsymbol{A}}_b \boldsymbol{X}_b \tilde{\boldsymbol{A}}_b^{\mathrm{T}} + \frac{1}{r_s} \tilde{\boldsymbol{A}}_s \boldsymbol{X}_s \tilde{\boldsymbol{A}}_s^{\mathrm{T}}. \tag{9}$$

To characterize the current output capacity of the RBS structure under different switching states, an indicator η is defined by the ratio of I_o to $\max(\boldsymbol{I}_b)$:

$$\eta = \frac{I_o}{\max(\boldsymbol{I}_b)}. \tag{10}$$

Finally the problem of finding the MAC can be formulated as

$$\max \eta(\boldsymbol{X}_s) \tag{11}$$

$$\text{s.t. } \max(\boldsymbol{I}_b) \leq I_m, \tag{12}$$

where I_m is the MAC of the battery.

However, it remains computationally difficult to solve Eq. (11) because of $\boldsymbol{Y}_n^{-1}$. On one hand, the introduction of nonlinear terms by $\boldsymbol{Y}_n^{-1}$ renders many methods in linear optimization unsuitable for this problem. On the other hand, the rank of Y_n is proportional to the number of batteries and switches, which can be very large for a large RBS, leading to a significant computational burden. As a result, intelligent algorithms that rely on evolution by iteration may face efficiency problems when dealing with a large RBS. To address this issue, the problem should be considered from the perspective of guiding the RBS to reconstruct as many parallel structures as possible. Consequently, a greedy algorithm based on the shortest path is proposed. The detailed implementation of this algorithm is presented in the following two subsections.

2.3 Shortest path

The path p used in this method is defined as the complete route that passes through one battery (or a consecutive series of batteries) and closed switches, connecting the anode v_1 to the cathode v_N of the RBS. By applying a penalty to the series-connected batteries on the path, where additional batteries imply a greater distance, the algorithm encourages the RBS to form parallel structures to the extent possible. In addition, to reduce the number of switches controlled during the reconstruction process, a penalty is also applied to the total number of switches on the path while ensuring the minimum number of batteries. Therefore, the distance ω of path p is

$$\omega(p) = N_s n_b(p) + n_s(p), \tag{13}$$

where N_s is the total number of switches in the system, and $n_b(p)$ and $n_s(p)$ are number of batteries and switches in path p, respectively. Moreover, the shortest path SP_i is defined as the path with the minimum ω for battery B_i:

$$SP_i = \arg\min_{p \in P_i} \omega(p), \tag{14}$$

where P_i is the set of all paths from v_1 to v_N that pass through directed edge i.

SP_i can be solved by the Dijkstra algorithm. The Dijkstra algorithm is a graph-search method that finds the shortest path between two given nodes in a weighted graph, efficiently solving the single-source shortest-path problem. Denoting the cathode and anode of battery B_i as v_i^- and v_i^+ respectively, then path p of battery B_i can be divided into three segments: $v_1 \to v_i^-$, $v_i^+ \to v_N$, and $v_i^- \to v_i^+$. $v_i^- \to v_i^+$ is the directed edge corresponding to battery B_i. With the Dijkstra algorithm, shortest paths for $v_1 \to v_i^-$ and $v_i^+ \to v_N$ can be calculated under the weights given in Eq. (13) and denoted $SP(v_i^- \to v_i^+)$ and $SP(v_i^+ \to v_N)$, respectively. Finally, SP_i for battery B_i is formed by the complete path, which consists of $SP(v_1 \to v_i^-)$, $v_i^- \to v_i^+$, and $SP(v_i^+ \to v_N)$.

2.4 Greedy algorithm

From the perspective of series vs parallel connections, integrating more batteries into the circuit through their shortest paths (SPs) results in more batteries connected in parallel, thereby increasing the total output current of the RBS. However, conflicts may arise between the SPs of different batteries. For instance, the SPs of two batteries might form a short-circuit RBS structure, which is not allowed. To address this issue, a greedy algorithm incorporates as many SPs as possible while satisfying the reconstruction requirements.

The algorithm (see pseudo-code in Algorithm 1) is illustrated in Fig. 3 and is summarized as follows: First, the SPs are obtained by using Eqs. (13) and (14) in conjunction with the Dijkstra search. Next, the matrix $\boldsymbol{A}$ is calculated using Eq. (1), and the initial N_{set} is set to N_b. The algorithm uses a dichotomy method to iteratively check until convergence different combinations of c_b batteries from N_b and updates N_{set}. For each combination, the algorithm constructs an effective solution if possible and calculates the currents I_o and $\boldsymbol{I}_b$ by using Eqs. (7) and (8). If the maximum current $\boldsymbol{I}_b$ is less than or equal to I_m, η is calculated by using Eq. (10), and the maximum η is updated accordingly. Finally, the algorithm outputs the maximum η once N_{set} converges.

3 Case Study

3.1 Structures and details

Currently, two types of RBS structures have been proposed by Visairo et al. [11] and Lawson et al. [17], both of which have seen real use. The primary goal of Visairo's structure (Fig. 4b) is to dynamically adjust the RBS output power. However, the isolation of unhealthy batteries is not sufficiently addressed in their work. Lawson et al. designed the RBS structure shown in Fig. 4a to isolate batteries. Although this structure easily isolates batteries, it cannot dynamically adjust the output current of the RBS. Based on the structures of Visairo and Lawson, this paper proposes the structure shown in Fig. 4c. By integrating the Visairo RBS structure into the Lawson RBS structure, the proposed structure not only has the flexibility to switch the batteries between series, parallel, and mixed series-parallel modes but also allows the isolation of highly degraded batteries from the RBS. ~~These four-battery RBS structures are investigated in~~

In the case study, ~~including the scenarios with random isolated batteries.~~ these RBS systems are investigated and compared: (a) three different structures (Figs. 4a–4c) with the same four batteries; (b) the same structure in Figs. 4c with two/four/six batteries; and (c) the four-battery structure in Figs. 4c with random isolated batteries. The greedy algorithm proposed in this work is also compared with the brute-force algorithm, SA, and GA to validate its effectiveness and efficiency. In order to adapt the two heuristic algorithms to the system's structure and scale, the number of the state neighbours of SA and the population size of GA are both set to $N_b \cdot N_s$, which increase with the number of batteries and switches in the system. The other algorithms' parameters are shown in Tab. 1.

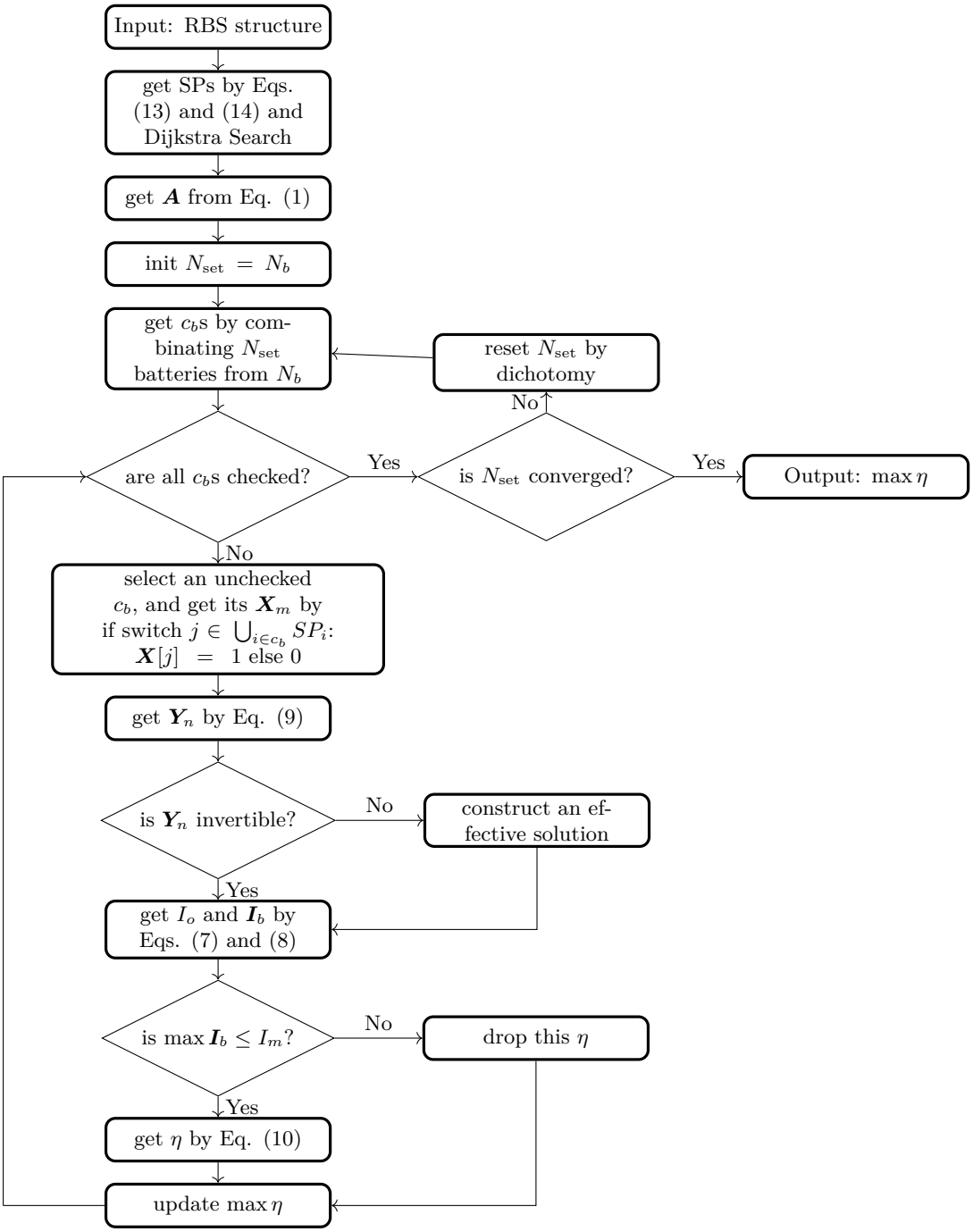

Figure 3: The computational flowchart of the MAC for a given RBS.

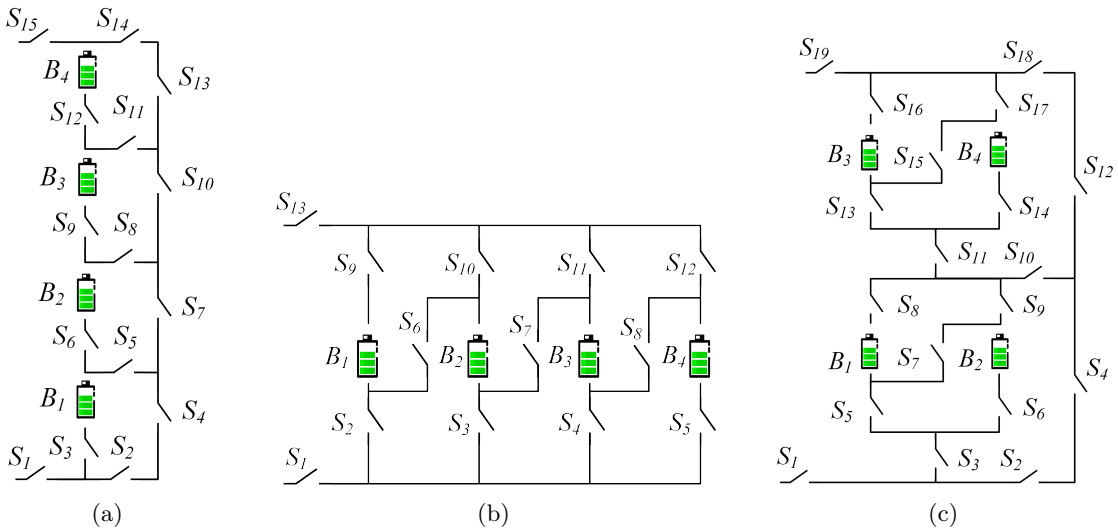

Figure 4: The four-battery RBS structures proposed by (a) Lawson [17], (b) Visairo [11], and (c) this paper.

Table 1: Algorithms parameters of SA and GA.

Algorithm/paramter	Value
SA/initial temperature	100
SA/final temperature	1
SA/cooling rate	0.95
GA/total generations	100
GA/crossover probability	0.8
GA/mutation probability	0.02

3.2 Result

~~As shown in Fig. 4c , the new RBS structure consists of fourbatteries and 19 switches. Figure ?? shows the corresponding directed graph, which is composed of 18 nodes and 43 edges. Batteries B_1, B_2, B_3, and B_4 are denoted by green directed edges in the graph, and the 19 switches are represented by gray directed edges with bidirectional arrows. The external electrical load is treated as a directed edge from the cathode of the RBS (i.e., node 18) to the anode (i.e., node 1), as indicated by the blue directed edge in the graph.~~

3.2.1 the shortest path

Using Eq. (13) and the Dijkstra algorithm, the SPs of the four batteries in the RBS ~~structure of Fig. 4c are highlighted in red in Figs. ?? and ??. Finally, the calculated~~ structures of Figs. 4a, 4b, and 4c are calculated and highlighted with difference colors in Figs. 5a, 5b, and 5c, respectively.

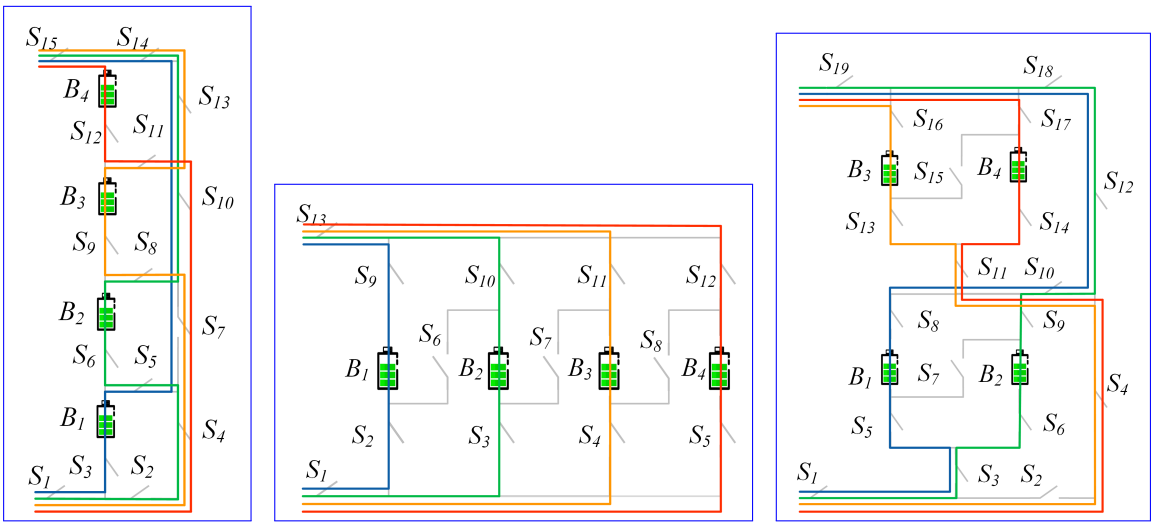

(a) (b) (c)

Figure 5: The SPs of the four batteries in the RBS structures of (a) Fig. 4a, (b) Fig. 4b, and (c) Fig. 4c.

3.2.2 three structures with four batteries

After obtaining the SPs, the MACs of the ~~structure in Fig. 4c are listed in Tab. 4 and shown in Fig. ??, as obtained by the greedy algorithm 1. Tab. 4~~three RBS structures with four batteries are calculated using the proposed greedy algorithm, and the results are shown in Tabs. 2, 3, and 4, each of which contains the states of the switches, the output current I_o, the battery current $\boldsymbol{I}_b$, and the ratio η ~~of the RBS structure with all batteries in good health when the RBS~~ when the system output reaches the MAC. ~~Fig. ?? presents the corresponding circuit, with the red highlight indicating that the current is flowing through the respective branches.~~

~~For the RBS structure in Fig. 4c, (a) its directed graph and the SPs (highlighted in red) of battery (b) B_1, (c) B_2, (d) B_3, and (e) B_4. (f) Circuit of RBS with its output reaching the MAC.~~

~~Calculated MAC for four-battery RBS structure in Fig. 4c. Structure Figure 4c with four batteries and 19 switches Switch on S_1,S_3,S_5,S_6,S_8,S_9,S_{10},S_{12},S_{18},S_{19} I_o $2u_b/(2R_o + r_b)$ $\boldsymbol{I}_b$ $[u_b/(2R_o + r_b), u_b/(2R_o + r_b),$ $\max \eta$ 2~~

~~Similarly, the results of the MAC calculation for the structures~~ The correspond switch-control schemes are shown as blue-highlighted electric current in Figs. ~~4a and 4b are listed in Tabs. 2 and 3~~6a, 6b, and 6c, respectively.

To verify and compare the ~~results from the~~ proposed greedy algorithm, we also used ~~a~~ the brute-force algorithm~~that~~, which iterates through all possible switch states, and the heuristic algorithms (SA and GA) to calculate the MAC of the same ~~three~~ RBSs. The final results of the brute-force algorithm are the same as the ~~results shown in Tabs. 4 3. The method uses~~ ones of the greedy algorithm~~to calculate 11, 11, and 1 reconfigured structures for the RBS structure in Figs. 4c, 4a, and 4b, respectively. For the same RBS, the method~~, which are shown in Tabs. 2, 3, and 4. But, the brute-force algorithm counts all possible switch states, which equates to ~~2^{19},~~ 2^{15}, ~~and~~ 2^{13}, and 2^{19} structures, respectively. The two heuristic algorithms' temporal evaluation of the objective values during the iteration process are shown in Figs. 7a, 7b, and 7c, respectively, compared with the proposed greedy algorithm. Comparing to the SA and GA, the proposed greedy algorithm solves the correct results with fewer iteration steps.

Table 2: MAC Calculating result of the four-battery RBS structure in Fig. 4a.

Structure	Figure 4a with 4 batteries and 15 switches
Switch ON	S_1,S_3,S_5,S_7,S_{10},S_{13},S_{14},S_{15}
I_o	$u_b/(R_o + r_b)$
$\boldsymbol{I}_b$	$[u_b/(R_o + r_b), 0, 0, 0]$
$\max \eta$	1

Table 3: MAC Calculating result of the four-battery RBS structure in Fig. 4b.

Structure	Figure 4b with 4 batteries and 13 switches
Switch ON	S_1,S_2,S_3,S_4,S_5,S_9,S_{10},S_{11},S_{12},S_{13}
I_o	$4u_b/(4R_o + r_b)$
$\boldsymbol{I}_b$	$[u_b/(4R_o + r_b), u_b/(4R_o + r_b), u_b/(4R_o + r_b), u_b/(4R_o + r_b)]$
$\max \eta$	4

~~Furthermore,the RBS with isolated batteries is taken into consideration and calculated. The MAC calculation~~

3.2.3 structures with different numbers of batteries

Table 4: Calculated MAC for four-battery RBS structure in Fig. 4c.

Structure	Figure 4c with four batteries and 19 switches
Switch on	S_1,S_3,S_5,S_6,S_8,S_9,S_{10},S_{12},S_{18},S_{19}
I_o	$2u_b/(2R_o+r_b)$
$\boldsymbol{I}_b$	$[u_b/(2R_o+r_b), u_b/(2R_o+r_b), 0, 0]$
$\max \eta$	2

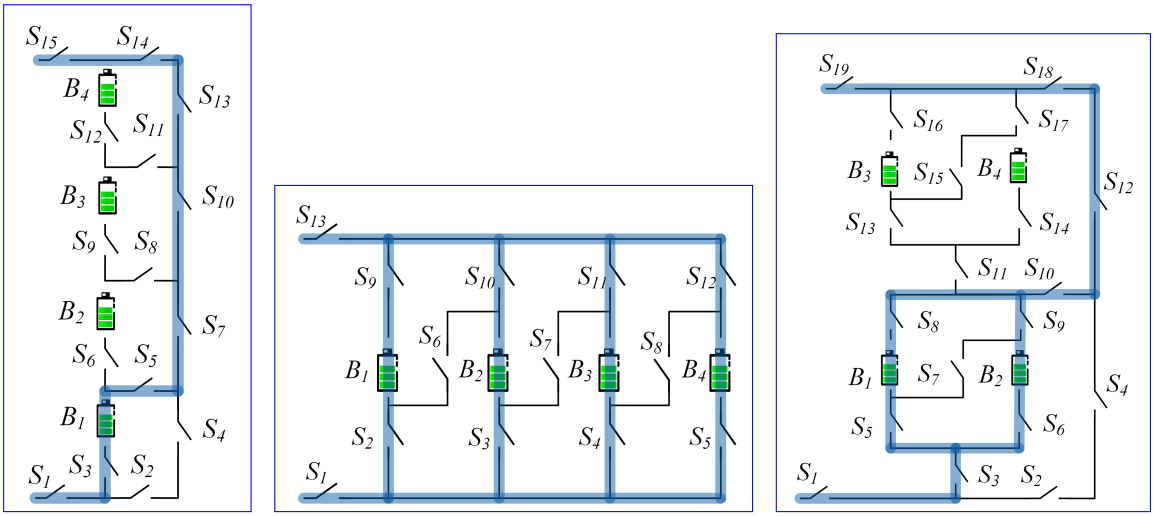

(a) (b) (c)

Figure 6: The RBSs' switch-control schemes with the output reaching the MAC.

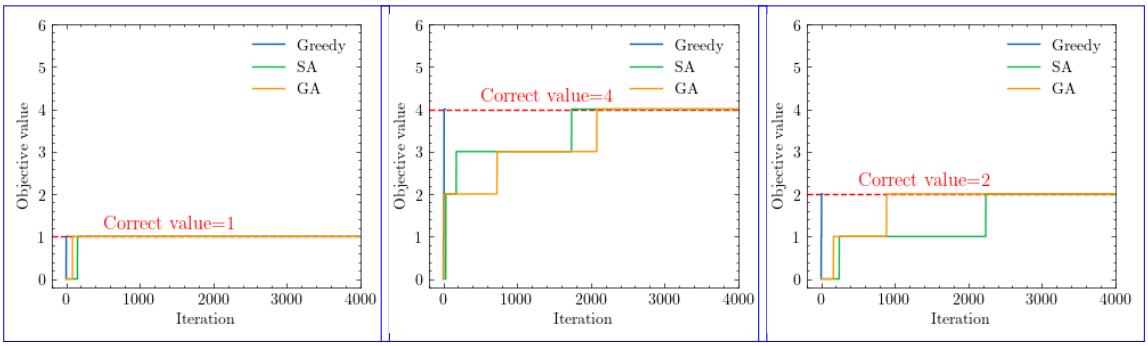

(a) (b) (c)

Figure 7: The temporal evolution of the objective values during the iteration process of calculating the RBS structures in (a) Fig. 4a, (b) Fig. 4b, and (c) Fig. 4c

We next examine the RBS configuration depicted in Fig. 4c, which consists of two, four, and six batteries. The results for the ~~three structures under study, with varying numbers of isolated batteries,~~ four-battery configuration are presented in Tab. ~~??. Figs. 10a–10d illustrate the corresponding~~ 4, Figs. 6c, and 7c. The structures and final switch-control schemes for the ~~new structureproposed in this paper under different conditions of isolated batteries~~two-battery and six-battery systems are illustrated in Figs. 8a and 8b, respectively. Furthermore, the temporal evolutions of the objective values throughout the iteration process are shown in Figs. 9a and 9b, respectively. The proposed greedy algorithm is still the one that converges the fastest and achieves the correct MAC. And the SA algorithm fails to obstain the correct MAC within the given iteration steps in the case of six-battery RBS structure.

~~Variation of MAC with the number of isolated batteries for different RBS structures, including the structure proposed by Lawson et al., Visairo et al., and the structure proposed in this paper.~~ ~~This paper Visairo Lawson 0~~

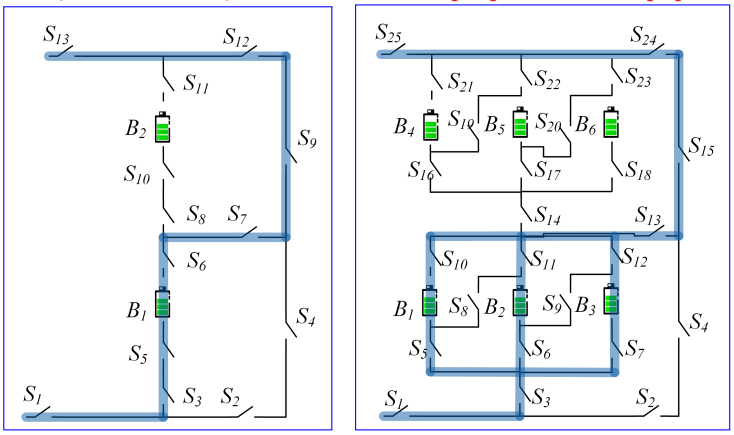

(a) (b)

Figure 8: The (a) two-battery and (b) six-battery RBSs' switch-control schemes with the output reaching the MAC.

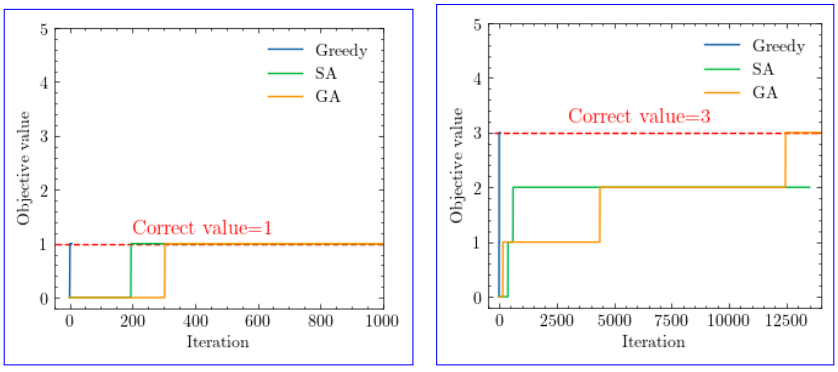

(a) (b)

Figure 9: The temporal variation of the objective values during the iteration process of calculating the RBS structures in (a) Fig. 8a and (b) Fig. 8b.

3.2.4 random isolated batteries

To assess the effectiveness of the proposed algorithm in the scenario of unhealthy batteries, the RBS with random isolated batteries is also taken into account and computed. In the case of the four-battery RBS structure depicted in Fig. 4c, there are four possible scenarios of isolated batteries: (a) only one unhealthy battery, (b) two unhealthy batteries that are separated in the two substructure, (c) two batteries located in the same substructure, and (d) three batteries. The resulting MAC (η) values for these four scenarios are 24 1 1 , 23 , 12 2[a] or , and 1[b] 2 1 3 1 1 1 , respectively. Furthermore, the corresponding switch-control schemes for these four scenarios are illustrated in Figs 10a–10d.

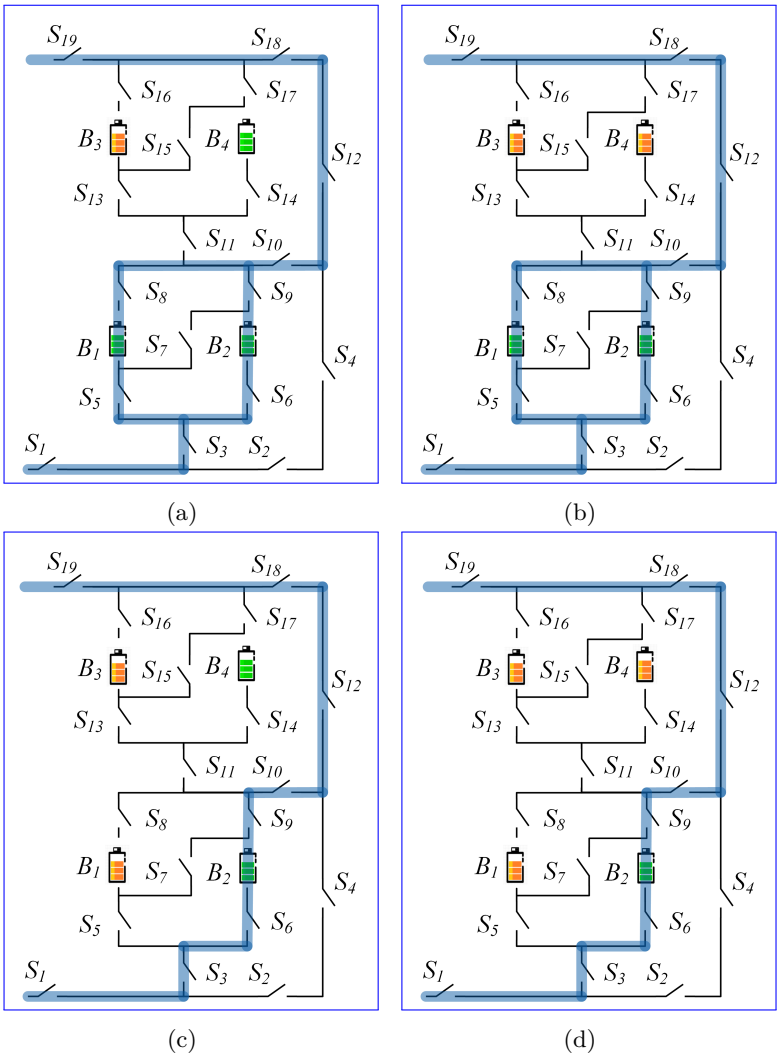

Figure 10: Circuit states of MACs when isolating (a) one, (b) two (best casein different substructures), (c) two (worst casein the same substructure), and (d) three batteries for the structure in Fig. 4c.

3.3 Discussion

~~Consider first the results~~

3.3.1 correctness of the results

The correctness of the outcomes provided by the proposed greedy algorithm will be discussed from two perspectives: circuit analysis and validation against the brute-force algorithm. Let's take the four-battery RBS structure shown in Fig. ~~?? and listed in Tab. 4.~~ 4c as an example. When B_1 and B_2 or B_3 and B_4 are connected in parallel, the RBS ~~outputs~~ produces the maximum current, which is $\eta = 2$ (i.e., twice the current output of a single battery in the RBS). Adding more batteries to the main circuit only ~~forms~~ creates a series structure and does not improve the MAC. Therefore, the ~~state of the switches given~~ switch-control scheme provided in Tab. 4 maximizes the RBS output current. ~~The~~ On the other hand, the brute-force method, which ~~go through~~ examines all possible switch states, also ~~gives the same result.~~ yields the same η. This indicates that the proposed greedy algorithm successfully identifies the MAC among all the potential reconfigured structures.

~~The literature contains no report on an algorithm for calculating the MAC of an RBS. The~~

3.3.2 advantages and disadvantages of our method

The proposed greedy algorithm possesses a significant advantage in terms of its effectiveness and efficiency. In this paper, it is compared with the brute-force algorithm, ~~which goes through~~ SA, and GA. While the brute-force algorithm ensures the correctness of the results by exploring all possible switch states, ~~is the most straightforward way to determine the MAC and is used as a benchmark for the~~ it comes at a high computational cost. The SA and GA are commonly used heuristic algorithms for addressing NP-hard problems. They selectively generate solutions for the switching states to maximize the objective value η. However, neither of these two algorithms can determine whether the current η represents the final MAC or if they should continue searching for better solutions. Moreover, as depicted in Figs. 7a–7c and Figs. 9a–9b, the SA and GA algorithms require more iterations to converge to the final solution compared to the proposed greedy algorithm. In contrast, the proposed greedy algorithm can identify the correct MAC in a shorter number of steps.

To further elaborate on the efficiency of our algorithm, we analyze the time complexity of both the brute-force algorithm and the greedy algorithm. If an RBS has N_b batteries and N_s switches and the corresponding directed graph has N nodes, 2^{N_s} iterations are required to traverse all reconfigured structures. Calculating each reconfigured structure using Eqs. (7)–(10) requires matrix inversion and matrix multiplication, which has a time complexity of $O(N^3 + 2N^2N_b + N^2N_s + NN_b^2)$. Therefore, the time complexity of the brute-force algorithm is $O\big((N^3 + 2N^2N_b + N^2N_s + NN_b^2)2^{N_s}\big)$. The greedy algorithm proposed in this paper requires that SP be found for each battery, which requires N_b iterations. Each SP can be obtained by several applications of Dijkstra's algorithms. Therefore, the total time complexity for calculating all SPs is $O\big(N_b(N_b+2N_s)\log_{10} N\big)$. According to Appendix 1, the RBS can reconfigure $C_{N_b}^{N_{\text{set}}}$ structures by selecting N_{set} batteries from N_b batteries, which gives $\sum_{N_{\text{set}}=1}^{N_b} C_{N_b}^{N_{\text{set}}}/N_b \approx 2^{N_b}N_b^{-1}$ on average. Thus, with the bisection method, the time complexity of the greedy algorithm is $O\big((N^3+2N^2N_b+N^2N_s+NN_b^2)2^{N_b}N_b^{-1}\log_{10} N_b + N_b(N_b+2N_s)\log_{10} N\big)$.

Based on currently proposed RBS structures [39, 40, 41, 42, 43, 44], the number N_b of batteries, N_s of switches, and N of nodes are quantitatively related as follows: $N_s \approx (3\text{–}5)N_b$, $N \approx N_s$. After simplifying, the time complexity of the method with greedy algorithm is $O(2^{N_b} N_s^2 \log_{10} N_b)$, while it is $O(2^{N_s} N_s^3)$ for the method with ~~brute force~~ brute-force algorithm. Therefore, as the RBS grows, especially in the number of switches, the greedy algorithm gains an advantage over the brute-force algorithm. This is confirmed by the number of structures required to determine the MAC in the previous section. Compared with the brute-force algorithm, the method based on the greedy algorithm is 3 000 to 48 000 times more efficient, which is theoretically $N_s 2^{N_s - N_b} \log_{10} N_b$ times according to the above time-complexity analysis. This benefits from two key points:

(1) The SPs guide the RBS to reconfigure reasonable structures rather than blindly going through all possible structures. This reduces the complexity from 2^{N_s} to 2^{N_b}, which is the main reason for the improvement in efficiency.

(2) The bisection method further accelerates this process, reducing the complexity from 2^{N_b} to $2^{N_b} N_B^{-1} \log_{10} N_b$.

~~However, the greedy algorithm proposed in this paper still contains~~

Furthermore, this approach has the capability to handle RBSs with arbitrary structures, which is another significant advantage of it. It is able to correctly calculate the MACs of RBSs with arbitrary structures, even when they have different variant batteries, or even random isolated batteries. Theoretically, each RBS structure can be transformed into the unique directed graph model using the methodology described in the Section II, and the MAC can subsequently be calculated using the proposed greedy algorithm. This finding has been supported in the previous subsection.

However, the suggested greedy algorithm still includes exponential terms in ~~the~~ its time complexity, ~~which means it may not be able to handle extremely large RBS structures having large N_b.~~ indicating that it struggles to perform at scale. Additionally, all batteries are assumed to be identical for the sake of simplification in the derivation. However, there may exist a small balancing current, which could introduce a minor bias to the MAC, due to variations in open-circuit voltage u_b and internal resistance r_b in reality. Nevertheless, the proposed greedy algorithm remains a viable choice for the RBS design and optimization in the early stage, and the issue of balancing current bias can be addressed by considering the variations in batteries and replacing the internal resistance with impedance when constructing the directed graph model.

3.3.3 application scenarios

Note that η is used as the objective function instead of I_o in solving for the MAC. This choice makes the resulting MAC more reasonable and applicable in practical scenarios. As shown in Tab. 4, I_o and $\boldsymbol{I}_b$ are functions of R_o, u_b, and r_b. However, when I_o is used as the objective function, even for the same RBS structure, the MAC solution and corresponding switch states could change due to different external electrical appliances. This would increase the difficulty and uncertainty of designing the RBS structure. To eliminate this problem, the ratio ~~$\eta = I_o / \max \boldsymbol{I}_b$~~ $\eta = I_o / \max(\boldsymbol{I}_b)$ is adopted as the objective function in our research. Recall that η reflects only the structure's ability

to output current, rather than the actual current outputing by the battery system. Assuming that the MAC of batteries in the RBS is I_m, the maximum output current of the RBS structure can be calculated as ηI_m by determining the value of η for the structure.

The method proposed in this paper facilitates the design of RBSs in the following ways: ~~Most~~ most currently proposed RBS structures [39, 40, 41, 42, 43, 44] have simple topological characteristics, so calculating the MACs is relatively straightforward, even intuitive. However, these simple structures do not always fully satisfy the requirements of complex applications, such as dynamically adapting the circuit to variable and random operating conditions or actively equalizing differences between batteries in the RBS. Moreover, isolating the batteries disrupts the original regularity and symmetry of the topology, which complicates the otherwise simple structure, and the maximum output current of the system becomes more challenging to obtain. In contrast, the proposed method calculates the MAC of arbitrary RBS structures, notably the complex and flexible RBS structures.

To illustrate this point, the MACs of ~~three RBS structures mentioned above~~ the RBS structure in Fig. 4c are calculated after isolating one or more of the batteries, as shown in ~~Tab. ??. Specifically, for the structure presented in Fig. 4c, the corresponding circuit states for the MACs when isolating one to three batteries are depicted in~~ Figs. 10a–10d. ~~This structure has two cases in which two~~ When a single battery is isolated, the RBS is still capable of outputting the maximum current, denoted as $\eta = 2$. When two batteries are isolated, there are two scenarios: one is ~~to isolate~~ isolating two batteries within the same substructure (~~Fig.~~ Figure 10b), ~~in which case~~ resulting in $\eta = 2$; the other is ~~to isolate~~ isolating one battery in each of the two substructures (~~Fig.~~ Figure 10c), ~~in which case~~ resulting in $\eta = 1$. ~~The results in Figs. 10a–10d show that the proposed method provides reasonable outcomes for isolating any number of batteries in any position. Furthermore, the output current for the three RBSs with isolated batteries is also shown in Tab. ??. For the structure proposed by Lawson et al., the MAC is independent of the number of isolated batteries. However, for Visairo's structure, the MAC decreases upon increasing the number of isolated batteries. Nevertheless, the MAC of the structure proposed in this work falls between the MACs of these two structures. This result indicates that the structure proposed in this paper has a larger MAC than Lawson's for the same number of batteriesand has a wider range of regulation of the output current~~If three batteries are isolated, the RBS can only output the current of a single battery, which is $\eta = 1$. Therefore, the battery management system can adjust the output current and control the RBS to reconfigure the corresponding structure based on the isolated batteries.

4 Conclusion

This paper proposes a pervasive and automated method to efficiently compute the MAC of an RBS. The method is implemented by a greedy algorithm combined with an improved directed graph model. Not only does the method provides the same global MAC calculation results as the ~~brute force~~ brute-force method, but it also ~~improves the calculation efficiency by 3 000 to 48 000 times for three RBS structures in the case study~~demonstrates superior computational efficiency compared to both the brute-force algorithm and the heuristic algorithms (SA and GA). Theoretically, for an RBS with N_s switches and N_b batteries, the efficiency of the proposed method is $N_s 2^{N_s - N_b} \log_{10} N_b$

times that of the brute-force method~~, which is mainly because of using~~. This is primarily due to the utilization of the batteries' SPs to guide the RBS to reconfigure reasonable structures rather than blindly going through all possible structures. ~~The main~~ Another advantage of this method is its ~~ability~~ capability to calculate the MAC of RBSs with arbitrary structures and variant batteries. Even in scenarios with random isolated batteries, the proposed method remains effective. This method ~~helps to fully tap the current output potential~~ facilitates the full utilization of the RBS~~,~~ ~~guide the RBS structure~~'s current output potential, guides the design and optimization ~~in the~~ of the RBS structure during the design stage, and ~~assist~~ assists in evaluating the ~~current-overload risk of the system~~ risk of current overload in practical applications.

5 Appendix

Algorithm 1: Get the max available currents of a certain RBS

Data: Directed graph model $G(V, E)$ of the RBS
Result: $\max \eta$
for $i \in E_b$ **do**
  $P_i \leftarrow \{path | \text{starts at } v_1 \text{ and ends at } v_n\}$;
  $SP_i \leftarrow p_i$ which has the minimum $\omega(p_i)$ among all $p_i \in P_i$.
end
get $\boldsymbol{A}$ by Eq. 1;
while *not yet determine* $\max \eta$ **do**
  $N_{\text{set}} \leftarrow$ number of setected SPs calculated by dichotomy;
  $C_b \leftarrow$ set of all combinations of N_{set} batteries from N_b;
  for $c_b \in C_b$ **do**
    $\boldsymbol{x}_s \leftarrow$ list of all switches' state: $x_s[j] = 1$ if $j \in \bigcup_{i \in c_b} SP_i$ else 0;
    $\boldsymbol{X} \leftarrow diag[1, 1, \cdots, 1, \boldsymbol{x}_s]$;
    get $\boldsymbol{Y}_n$ by Eq. 9;
    if $\boldsymbol{Y}_n$ *is invertible* **then**
      pass
    else
      construct an effective solution
    end
    get I_o by Eq. 7;
    get $\boldsymbol{I}_b$ by Eq. 8;
    if $\max(\boldsymbol{I}_b) \leq I_m$ **then**
      $\eta \leftarrow I_o / \max(\boldsymbol{I}_b)$;
    else
      break
    end
  end
end

Acknowledgments

Author Contributions

B. Xu conceived the main idea, formulated the overarching research goals and aims, designed the algorithm, and reviewed and revised the manuscript. G. Hua developed and analyzed the model, implemented the code and supporting algorithms, and wrote the initial draft. C. Qian provided critical review, commentary, and revisions. Q. Xia contributed to shaping the research, analysis, and manuscript. B. Sun conducted the research and investigation process. Y. Ren secured the funding and supervised the project. Z. Wang verified the results and provided necessary resources.

~~Funding~~

~~This work was supported by the National Natural Science Foundation of China (NSFC, No.52075028).~~

Conflicts of Interest

The authors declare that there is no conflict of interest regarding the publication of this article.

Data Availability

This work does not require any data to be declared or publicly disclosed.

References

[1] Yuqing Yang, Stephen Bremner, Chris Menictas, and Merlinde Kay. Battery energy storage system size determination in renewable energy systems: A review. *Renewable and Sustainable Energy Reviews*, 91:109–125, August 2018.

[2] Luanna Maria Silva de Siqueira and Wei Peng. Control strategy to smooth wind power output using battery energy storage system: A review. *Journal of Energy Storage*, 35:102252, March 2021.

[3] Eugene Schwanbeck and Penni Dalton. International Space Station Lithium-ion Batteries for Primary Electric Power System. In *2019 European Space Power Conference (ESPC)*, pages 1–1. IEEE, September 2019.

[4] Lihua Zhang. Development and Prospect of Chinese Lunar Relay Communication Satellite. *Space: Science & Technology*, 2021, January 2021.

[5] Jaephil Cho, Sookyung Jeong, and Youngsik Kim. Commercial and research battery technologies for electrical energy storage applications. *Progress in Energy and Combustion Science*, 48:84–101, June 2015.

[6] Naixing Yang, Xiongwen Zhang, BinBin Shang, and Guojun Li. Unbalanced discharging and aging due to temperature differences among the cells in a lithium-ion battery pack with parallel combination. *Journal of Power Sources*, 306:733–741, February 2016.

[7] Fei Feng, Xiaosong Hu, Lin Hu, Fengling Hu, Yang Li, and Lei Zhang. Propagation mechanisms and diagnosis of parameter inconsistency within Li-Ion battery packs. *Renewable and Sustainable Energy Reviews*, 112:102–113, September 2019.

[8] J. A. Jeevarajan and C. Winchester. Battery Safety Qualifications for Human Ratings. *Interface magazine*, 21(2):51–55, January 2012.

[9] Daniel Vázquez Pombo. A Hybrid Power System for a Permanent Colony on Mars. *Space: Science & Technology*, 2021, January 2021.

[10] Weiji Han, Torsten Wik, Anton Kersten, Guangzhong Dong, and Changfu Zou. Next-Generation Battery Management Systems: Dynamic Reconfiguration. *IEEE Industrial Electronics Magazine*, 14(4):20–31, December 2020.

[11] H. Visairo and P. Kumar. A reconfigurable battery pack for improving power conversion efficiency in portable devices. In *2008 7th International Caribbean Conference on Devices, Circuits and Systems*, pages 1–6. IEEE, April 2008.

[12] Song Ci, Ni Lin, and Dalei Wu. Reconfigurable battery techniques and systems: A survey. *IEEE Access*, 4:1175–1189, 2016.

[13] Nejmeddine Bouchhima, Matthias Gossen, Sascha Schulte, and Kai Peter Birke. Lifetime of self-reconfigurable batteries compared with conventional batteries. *Journal of Energy Storage*, 15:400–407, 2018.

[14] Song Ci, Jiucai Zhang, Hamid Sharif, and Mahmoud Alahmad. A novel design of adaptive reconfigurable multicell battery for power-aware embedded networked sensing systems. In *IEEE GLOBECOM 2007-IEEE Global Telecommunications Conference*, pages 1043–1047. IEEE, 2007.

[15] Jan Engelhardt, Tatiana Gabderakhmanova, Gunnar Rohde, and Mattia Marinelli. Reconfigurable stationary battery with adaptive cell switching for electric vehicle fast-charging. In *2020 55th International Universities Power Engineering Conference (UPEC)*, pages 1–6, 2020.

[16] Jan Engelhardt, Jan Martin Zepter, Tatiana Gabderakhmanova, Gunnar Rohde, and Mattia Marinelli. Double-string battery system with reconfigurable cell topology operated as a fast charging station for electric vehicles. *Energies*, 14(9):2414, 2021.

[17] Barrie Lawson. A Software Configurable Battery. *EVS26 International Battery, Hybrid and Fuel Cell Electric Vehicle Symposium*, 2012.

[18] Liang He, Linghe Kong, Siyu Lin, Shaodong Ying, Yu Gu, Tian He, and Cong Liu. Reconfiguration-assisted charging in large-scale lithium-ion battery systems. In *2014*

ACM/IEEE International Conference on Cyber-Physical Systems (ICCPS), pages 60–71. IEEE, 2014.

[19] Hahnsang Kim and Kang G Shin. On dynamic reconfiguration of a large-scale battery system. In *2009 15th IEEE Real-Time and Embedded Technology and Applications Symposium*, pages 87–96. IEEE, 2009.

[20] Weiji Han and Anton Kersten. Analysis and Estimation of the Maximum Circulating Current during the Parallel Operation of Reconfigurable Battery Systems. In *2020 IEEE Transportation Electrification Conference & Expo (ITEC)*, pages 229–234. IEEE, June 2020.

[21] Jan Engelhardt, Jan Martin Zepter, Tatiana Gabderakhmanova, Gunnar Rohde, and Mattia Marinelli. Double-String Battery System with Reconfigurable Cell Topology Operated as a Fast Charging Station for Electric Vehicles. *Energies*, 14(9):2414, 2021.

[22] Weiji Han, Anton Kersten, Changfu Zou, Torsten Wik, Xiaoliang Huang, and Guangzhong Dong. Analysis and estimation of the maximum switch current during battery system reconfiguration. *IEEE Transactions on Industrial Electronics*, 69(6):5931–5941, 2021.

[23] Lidiya Komsiyska, Tobias Buchberger, Simon Diehl, Moritz Ehrensberger, Christian Hanzl, Christoph Hartmann, Markus Hölzle, Jan Kleiner, Meinert Lewerenz, Bernhard Liebhart, Michael Schmid, Dominik Schneider, Sascha Speer, Julia Stöttner, Christoph Terbrack, Michael Hinterberger, and Christian Endisch. Critical Review of Intelligent Battery Systems: Challenges, Implementation, and Potential for Electric Vehicles. *Energies*, 14(18):5989, 2021.

[24] Luis D. Couto and Michel Kinnaert. Partition-based Unscented Kalman Filter for Reconfigurable Battery Pack State Estimation using an Electrochemical Model. In *2018 Annual American Control Conference (ACC)*, pages 3122–3128. IEEE, June 2018.

[25] Anton Kersten, Manuel Kuder, Weiji Han, Torbjorn Thiringer, Anton Lesnicar, Thomas Weyh, and Richard Eckerle. Online and On-Board Battery Impedance Estimation of Battery Cells, Modules or Packs in a Reconfigurable Battery System or Multilevel Inverter. In *IECON 2020 The 46th Annual Conference of the IEEE Industrial Electronics Society*, pages 1884–1891. IEEE, October 2020.

[26] Michael Schmid, Emanuel Gebauer, Christian Hanzl, and Christian Endisch. Active Model-Based Fault Diagnosis in Reconfigurable Battery Systems. *IEEE Transactions on Power Electronics*, 36(3):2584–2597, March 2021.

[27] Jan Kacetl, Jingyang Fang, Tomas Kacetl, Nima Tashakor, and Stefan Goetz. Design and Analysis of Modular Multilevel Reconfigurable Battery Converters for Variable Bus Voltage Powertrains. *IEEE Transactions on Power Electronics*, 38(1):130–142, January 2023.

[28] Feng Yang, Fei Gao, Baochang Liu, and Song Ci. An Adaptive Control Framework for Dynamically Reconfigurable Battery Systems Based on Deep Reinforcement Learning. *IEEE Transactions on Industrial Electronics*, 69(12):12980–12987, December 2022.

[29] Weiji Han, Changfu Zou, Liang Zhang, Quan Ouyang, and Torsten Wik. Near-Fastest Battery Balancing by Cell/Module Reconfiguration. *IEEE Transactions on Smart Grid*, 10(6):6954–6964, November 2019.

[30] Xinghua Liu, Guoyi Chang, Jiaqiang Tian, Zhongbao Wei, Xu Zhang, and Peng Wang. Flexible path planning-based reconfiguration strategy for maximum capacity utilization of battery pack. *Journal of Energy Chemistry*, 86:362–372, November 2023.

[31] Si-Zhe Chen, Yule Wang, Guidong Zhang, Le Chang, and Yun Zhang. Sneak Circuit Theory Based Approach to Avoiding Short-Circuit Paths in Reconfigurable Battery Systems. *IEEE Transactions on Industrial Electronics*, 68(12):12353–12363, 2021.

[32] Kailong Liu, Zhongbao Wei, Chenghui Zhang, Yunlong Shang, Remus Teodorescu, and Qing-Long Han. Towards Long Lifetime Battery: AI-Based Manufacturing and Management. *IEEE/-CAA Journal of Automatica Sinica*, 9(7):1139–1165, July 2022.

[33] Morteza Mollajafari. An efficient lightweight algorithm for scheduling tasks onto dynamically reconfigurable hardware using graph-oriented simulated annealing. *Neural Computing and Applications*, 35(24):18035–18057, August 2023.

[34] Liang He, Linghe Kong, Siyu Lin, Shaodong Ying, Yu Gu, Tian He, and Cong Liu. Reconfiguration-assisted charging in large-scale Lithium-ion battery systems. In *2014 ACM/IEEE International Conference on Cyber-Physical Systems (ICCPS)*, pages 60–71. IEEE, April 2014.

[35] Zoltan Mark Pinter, Dimitrios Papageorgiou, Gunnar Rohde, Mattia Marinelli, and Chresten Traholt. Review of Control Algorithms for Reconfigurable Battery Systems with an Industrial Example. In *2021 56th International Universities Power Engineering Conference (UPEC)*, pages 1–6, August 2021.

[36] Liang He, Lipeng Gu, Linghe Kong, Yu Gu, Cong Liu, and Tian He. Exploring Adaptive Reconfiguration to Optimize Energy Efficiency in Large-Scale Battery Systems. In *2013 IEEE 34th Real-Time Systems Symposium*, pages 118–127, December 2013.

[37] Hongwen He, Rui Xiong, Xiaowei Zhang, Fengchun Sun, and JinXin Fan. State-of-Charge Estimation of the Lithium-Ion Battery Using an Adaptive Extended Kalman Filter Based on an Improved Thevenin Model. *IEEE Transactions on Vehicular Technology*, 60(4):1461–1469, May 2011.

[38] S.M. Mousavi G. and M. Nikdel. Various battery models for various simulation studies and applications. *Renewable and Sustainable Energy Reviews*, 32:477–485, April 2014.

[39] Song Ci, Jiucai Zhang, Hamid Sharif, and Mahmoud Alahmad. A Novel Design of Adaptive Reconfigurable Multicell Battery for Power-Aware Embedded Networked Sensing Systems. In *IEEE GLOBECOM 2007-2007 IEEE Global Telecommunications Conference*, pages 1043–1047, November 2007.

[40] Mahmoud Alahmad, Herb Hess, Mohammad Mojarradi, William West, and Jay Whitacre. Battery switch array system with application for JPL's rechargeable micro-scale batteries. *Journal of Power Sources*, 177(2):566–578, March 2008.

[41] Hahnsang Kim and Kang G. Shin. Dependable, efficient, scalable architecture for management of large-scale batteries. In *Proceedings of the 1st ACM/IEEE International Conference on Cyber-Physical Systems*, ICCPS '10, pages 178–187, New York, NY, USA, April 2010. Association for Computing Machinery.

[42] Younghyun Kim, Sangyoung Park, Yanzhi Wang, Qing Xie, Naehyuck Chang, Massimo Poncino, and Massoud Pedram. Balanced reconfiguration of storage banks in a hybrid electrical energy storage system. In *2011 IEEE/ACM International Conference on Computer-Aided Design (ICCAD)*, pages 624–631, November 2011.

[43] Taesic Kim, Wei Qiao, and Liyan Qu. A series-connected self-reconfigurable multicell battery capable of safe and effective charging/discharging and balancing operations. In *2012 Twenty-Seventh Annual IEEE Applied Power Electronics Conference and Exposition (APEC)*, pages 2259–2264, February 2012.

[44] Liang He, Linghe Kong, Siyu Lin, Shaodong Ying, Yu Gu, Tian He, and Cong Liu. Reconfiguration-assisted charging in large-scale Lithium-ion battery systems. In *2014 ACM/IEEE International Conference on Cyber-Physical Systems (ICCPS)*, pages 60–71, April 2014.